Max-Planck-Institut für Meteorologie
Max Planck Institute for Meteorology

Report No. 352

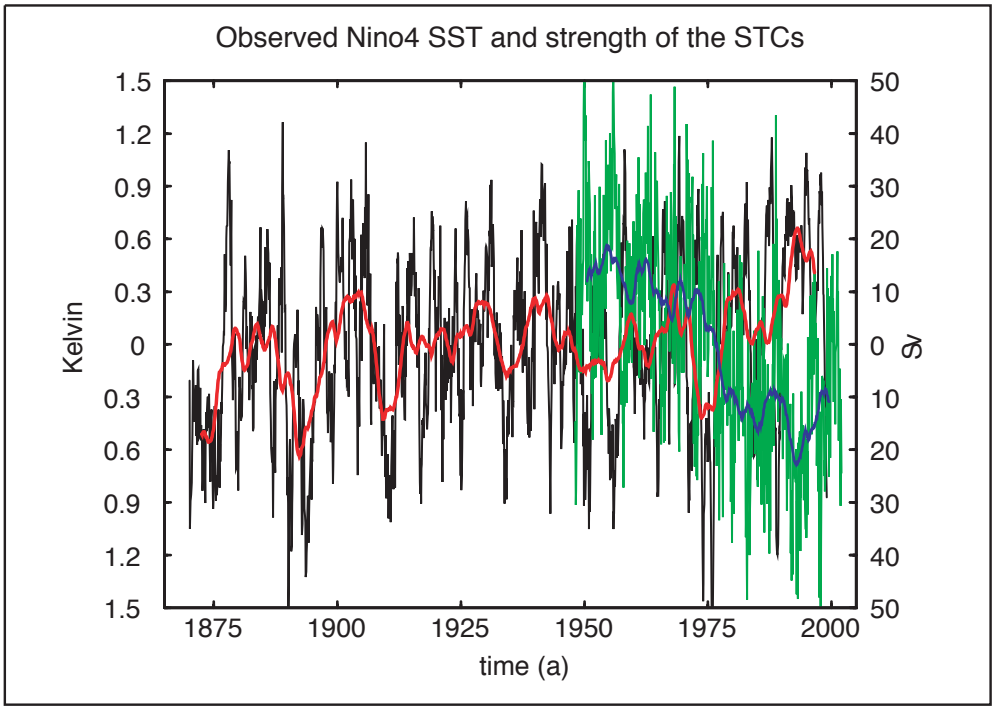

Tropical Pacific Decadal Variability and the Subtropical-Tropical Cells

by

Katja Lohmann · Mojib Latif

Hamburg, March 2004

Authors

Katja Lohmann	Max-Planck-Institut für Meteorologie Hamburg, Germany
Mojib Latif	Institut für Meereskunde Kiel, Germany

Max-Planck-Institut für Meteorologie
Bundesstrasse 53
D - 20146 Hamburg
Germany

Tel.: +49-(0)40-4 11 73-0
Fax: +49-(0)40-4 11 73-298
e-mail: <name>@dkrz.de
Web: www.mpimet.mpg.de

Tropical Pacific Decadal Variability and the Subtropical-Tropical Cells

Katja Lohmann
Max-Planck-Institut für Meteorologie
Bundesstr. 53, 20146 Hamburg, Germany
email: katja.lohmann@dkrz.de

and

Mojib Latif
Institut für Meereskunde
Düsternbrooker Weg 20, 24105 Kiel, Germany
email: mlatif@ifm-geomar.de

(submitted to Journal of Climate)

ISSN 0937-1060

Abstract

We have analyzed the decadal-scale variability in the Tropical Pacific by means of observations and numerical model simulations. The two leading modes of the sea surface temperature (SST) variability in the central western Pacific are a decadal mode with a period of about 10 years and the ENSO mode with a dominant period of about four years. The SST anomaly pattern of the decadal mode is ENSO-like. The decadal mode, however, explains most variance in the western equatorial Pacific and off the equator. A simulation with an ocean general circulation model (OGCM) forced by reanalysis data is used to explore the origin of the decadal mode. It is found that the variability of the shallow subtropical-tropical overturning cells (STCs) is an important factor in driving the decadal mode. This is supported by results from a multi-century integration with a coupled ocean-atmosphere general circulation model (CGCM) that realistically simulates Tropical Pacific decadal variability. Finally, the sensitivity of the STCs to greenhouse warming is discussed by analyzing the results of a scenario integration with the same CGCM.

1. Introduction

The sea surface temperature (SST) in the Tropical Pacific exhibits pronounced decadal-scale variability. *Trenberth and Hurrell (1994)* and *Graham (1994)* describe this decadal variability in detail and conclude that it originates in the Tropical Pacific itself. *Gu and Philander (1997, in the following named GP97)*, on the other hand, propose that the decadal variability in the Tropical Pacific is part of a cycle that involves the Tropics and the Extratropics, in which the mean advection of temperature anomalies from the Extratropics to the Tropics plays a crucial role and determines the decadal timescale. *Barnett et al. (1999)* offers an alternative explanation. They argue that decadal variability in the North Pacific reaches into the Tropics and drives part of the tropical decadal variability through atmospheric teleconnections.

Several other studies investigate the influence of the shallow subtropical-tropical overturning cells (STCs, e.g. *McCreary and Lu (1994), Liu (1994)*) on the SST variability in the Tropical Pacific . These mainly wind driven cells appear in the zonal integral as closed cells with an upwelling at the equator, a poleward Ekman transport at the surface, subduction in the subtropics and an equatorward flow within the thermocline. It is unclear, however, if these cells are really closed. *Johnson (2001)*, for instance, suggests that the poleward surface limb does not reach the subduction areas in the east. The maximum strength of the cells is found close to the equator.

These small recirculation cells are often referred to as tropical cells (TCs, *Lu et al. (1998)*). Their appearance can depend on the way the streamfunction is calculated (*Hazeleger et al. (2003)*). The proposed influence of the STCs onto the SST is due to (1) the spin-up and -down of the cells leading to anomalies in the equatorward transport and upwelling strength of cold subsurface water and (2) due to the advection of temperature anomalies by the mean flow from the subtropical subduction areas. These two mechanisms are referred to as (1) $v' \overline{T}$ and (2) $\overline{v} T'$ mechanism, respectively.

The first mechanism was suggested by *Kleeman et al. (1999)* from analysis of the tropical decadal variability simulated by a 3 1/2 layer ocean model coupled to a statistical atmosphere. Further supporting model studies were performed by *Klinger et al. (2002)* and *Solomon et al. (2003)* using the same ocean model and by *Nonaka et al. (2002)* who used an ocean general circulation model (OGCM) forced by observed wind stresses. *Merryfield and Boer (2004, submitted)* analyzed a coupled general circulation model (CGCM) simulation and found the $v' \overline{T}$ mechanism to be the dominating one. *McPhaden and Zhang (2002)* reported by investigating hydrographic data and observed SST that the warming of the Tropical Pacific in the last decades was associated with a decrease in the strength of the STCs.

The second mechanism was described by *GP97* using a simple box model, by *Zhang et al. (1998)* analyzing the Levitus data and by *Giese et al. (2002)* using an OCGM. *Schneider et al. (1999)*, however, suggest from OGCM experiments that the subducted temperature anomalies from the subtropics do not affect the equatorial SST. This is supported by *Hazeleger et al. (2001)* who did not find any propagation of temperature anomalies to the equator in a combined model and observational study. In a recent study, *Boccaletti et al. (2004, submitted)* propose diabatic processes instead. *Yang and Liu (2004, submitted)* find both mechanisms of importance in their CGCM experiments.

In this study, we use observed SSTs in combination with an ocean general circulation model forced by NCEP reanalysis data as well as a coupled atmosphere-ocean general circulation model to investigate the decadal variability in the Tropical Pacific. Special attention is given to the role of the subtropical-tropical cells. The paper is organized as follows: Chapter 2 gives a short overview of the data. The observed decadal variability in the Tropical Pacific SST and its relationship to the STCs (from an NCEP forced ocean model) is described in chapters 3 and 4, respectively. Chapter 5 discusses the results from the coupled model experiments, and the main conclusions are given in chapter 6.

2. Data

The observed SST is taken from the Hadley Centre Ice and Sea Surface Temperature dataset HadISST1.1 encompassing the years 1870 to 1998 (*Rayner et al. (2003)*). To get further insight into the dynamics of the observed SST variability we analyze a 54 year integration of the ocean general circulation model MPI-OM1 forced by the NCEP-NCAR reanalysis for the years 1948 to 2001. The MPI-OM1 model, described by *Marsland et al. (2003)*, is a new version of the Hamburg Ocean Primitive Equation model HOPE using a C-grid and orthogonal curvilinear co-ordinates. The OGCM was used by *Latif et al. (2004)* in coupled mode using the atmosphere model ECHAM5 to study the multi-decadal variability in the North Atlantic. The horizontal resolution amounts to about 3^o x 3^o. The grid has a meridional refinement at the equator, with 0.5^o resolution between 10^oS and 10^oN. Vertically, 23 levels were used, of which 10 are in the upper 300 meters. The surface heatflux was not taken from the NCEP reanalysis, but calculated according to Bulk formulae (see *Marsland et al. (2003)*). Initial conditions were obtained from an extended-range integration with climatological forcing.

Additionally, we analyze a 300 year control integration of the coupled general circulation model ECHAM4/OPYC3. The atmosphere model is ECHAM4 (*Roeckner et al., 1996*) with 19 vertical levels and a horizontal resolution of T42 corresponding to about 2.8^o x 2.8^o. The OPYC model (*Oberhuber, 1993*) is an isopycnal ocean model based on the primitive equations and has an embedded mixed layer model. The OGCM has a horizontal resolution of 2.8^o x 2.8^o with a gradual meridional refinement in the subtropical/tropical region and a meridional resolution of 0.5^o in the equatorial region. It was run with 11 vertical density layers, and the output was interpolated onto fixed depth levels, 48 for the meridional overturning (18 in the upper 300 meters) and 10 for the other variables (5 in the upper 300 meters). We analyze additionally the results of a 240 year long greenhouse warming simulation (*Roeckner et al., 1999*). The increase in CO_2 is prescribed from observations from 1860 up to present and follows the IPCC 1992a scenario until 2100. All data used in this study are monthly values with the mean annual cycle removed.

3. Observed variability in Niño4 SST

Observations indicate that the decadal SST variability is particularly strong in the western central equatorial Pacific (e.g. *Trenberth and Hurrell (1994), Graham (1994)*). We have chosen therefore the Niño4 region (160^oE-150^oW, 5^oN-5^oS) to begin our analysis of the decadal variability. Figure 1 shows the observed sea surface temperature anomalies (SSTAs) averaged over

the Niño4 region from 1870 onwards. The timeseries exhibits rather strong decadal fluctuations with strong interannual variability superimposed. In order to highlight the decadal variability a five year running mean is also shown. It is interesting that the relatively strong change in the mid-seventies is not unusual in the context of the last 130 years. We note also that there is a rather strong trend in the Niño4 SSTA timeseries during the last few decades.

We decomposed the monthly Niño4 SSTA timeseries by means of a singular spectrum analysis (SSA). The reconstructed Niño4 SSTA timeseries using the first two SSA modes (pairs) are shown in Figure 2. The leading temporal mode, accounting for about 25% of the variance of the Niño4 index, has a quasi-decadal timescale (Figure 2a). It closely resembles the low-pass filtered curve (five year running mean) shown in Figure 1. The second most energetic mode (Figure 2b) corresponds to the well-known interannual variability associated with the El Niño/ Southern Oscillation (ENSO) phenomenon. It explains about 20% of the variance. We note that the warming trend in the western equatorial Pacific seen in Figure 1 projects only onto the decadal, but not onto the ENSO mode. The ENSO mode also exhibits pronounced decadal-scale variability, which is seen as an amplitude modulation. The processes behind this amplitude modulation are still highly controversial. No clear trend in the ENSO amplitude is seen in the corresponding SSA reconstruction, so that the interpretation of the climate change in the Tropical Pacific observed during the recent decades is as follows: The more frequent and stronger El Niño events during the 1990s is probably due to the positive swing in the decadal mode, which simply shifts the "working point" for ENSO towards the positive side (see also *Latif et al. (1997)*). This means that the El Niños of 1982/1983 and 1997/1998 may have become record events, because there is an upward trend in the decadal mode, and since the decadal mode was additionally in a positive extreme phase. Thus, one may argue that the background conditions on which ENSO operates have changed, but ENSO itself did not.

Next, we computed by means of linear regression the spatial structures associated with the two leading temporal modes, as expressed by the corresponding reconstructions (Figure 2). The two regression patterns and the associated explained variances are shown in Figures 3 and 4, respectively. The decadal mode is El Niño-like (Figure 3a), as described in other papers (e.g. *Zhang et al. (1997)*). However, there are important differences to the canonical El Niño structure. The regression pattern for the decadal mode is broader in the meridional direction and stronger in the western than in the eastern equatorial Pacific. Near the dateline, the regression coefficients amount to about 0.3^{o}C per standard deviation of the decadal mode timeseries (Figure 2a).

The interannual mode shows the typical El Niño structure, with strongest anomalies in the eastern and central equatorial Pacific (Figure 3b). Maximum regression coefficients reach 0.4^{o}C per standard deviation of the ENSO mode timeseries (Figure 2b). The associated explained variances also differ between the two modes. The decadal mode (Figure 4a) shows a horseshoe-like structure in the explained variances, with maximum values in the western equatorial Pacific and off the equator, but low explained variances in the eastern equatorial Pacific. The interannual mode (Figure 4b), on the other hand, explains most variance at the equator. Please note that the largest explained variances must occur in the central Niño4 region, since the corresponding SSTA timeseries was used in the SSA.

4. Relation of the decadal mode to the STCs

We discuss now the relationship between the observed decadal SST variations in the Niño4 region and the subtropical-tropical cell (STC) variability derived from the NCEP forced ocean model integration. An index for the strength of the cells was defined by taking for each timestep psi_{max} - psi_{min} , where *psi* is the meridional overturning in the upper 250 meters and the subtropical-tropical range (the overturning is negative for the southern cell). To account for the fact that the surface branches of the cells are spinning up and down quicker than the pycnocline branches (*Liu (1998), Klinger et al. (2002), Merryfield and Boer (2004, submitted)*), the decadal STC variability discussed in this study is determined from overturning data with a five year running mean applied. In Figure 1, both the raw and the low-pass filtered STC indices are shown in addition to the Niño4 SSTA timeseries. The chosen index mainly describes the equatorial part (the TCs) of the STCs. The dependance on latitude is discussed below (Figures 5 and 6).

We now concentrate on the decadal timescale and consider quantities which were smoothed by a 5-year running mean filter. The STC and Niño4 SSTA timeseries are strongly anticorrelated, so that anomalously warm Niño4 SST goes along with anomalously weak overturning cells. The correlation coefficient between the two (low-pass filtered) timeseries amounts to -0.7, with the overturning leading by a few months (Figure 5a). The time lag indicates that the overturning cell variability is indeed driving the decadal SST fluctuations in the Niño4 region. Considering the northern and the southern cell separately, the lag is about 2 month for the southern and 7 month for the northern cell. The associated spatial correlation pattern between the decadal cell strength index (blue curve in Figure 1) and the observed SSTs closely resembles that shown in Figure 4a in the Tropical Pacific (the equatorial horseshoe-like structure), indicating that the influence of the cells is higher in the western than in the eastern equatorial Pacific.

The most striking feature in our OGCM simulation is the spin-down of the cells over the last 50 years which goes along with a warming of the Niño4 SST. *Wu and Xie (2003*) call for caution in studies of the Tropical Pacific variability based on NCEP forced ocean models due to differences in NCEP and COADS winds. This trend, however, has been also found by *McPhaden and Zhang (2002)* who used hydrographic data. They determined the pycnocline transports at about 9^o latitude and computed the convergence of the transports to obtain a measure of the STC strength. Furthermore, the trend is simulated in each individual member of an ensemble of integrations with the MPI-OM1 model, run with a coarser horizontal (but higher vertical) resolution, in which the initial conditions were varied (not shown). This was achieved by conducting ten integrations with identical forcing. The initial conditions for each ensemble member were taken from the state simulated at the end of the preceeding member. It is therefore unlikely that the strong downward trends seen in our model simulations arise from problems associated with the OGCM initialization.

To investigate the influence of the off-equatorial regions on the western equatorial SST variability we determine the cross-correlation functions (Figure 5) between the low-pass filtered Niño4 SSTA and indices of the STC strength computed from different latitudes. For instance, "10^o latitude" in Figure 5b means that we computed ($psi_{max}(10^oN)$-$psi_{min}(10^oS)$). Again, the off-equatorial cell indices have been calculated from overturning data to which a five year running mean was applied. With increasing distance from the equator the correlation coefficient decreases and the lag between STC and SST anomalies increases. At 10^o latitude (Figure 5b), the largest correlation coefficient amounts to -0.6 with the overturning leading by about 15 months. *Nonaka et al. (2002)* found a lag of about 2 years between the equatorial temperature anomalies simulated by an ocean model forced by only equatorial winds and those from an ocean model forced with no equatorial winds. Poleward of 15^o latitude, the correlation drops to a value close to the significance level (-0.44 according to a t-test). The fact that the trend in the STC strength seen in Figure 1 vanishes at about 15^o latitude might contribute to the low correlations.

Figure 6 shows the pattern for the regression of the meridional overturning streamfunction onto the decadal Niño4 SST mode (Figure 2a). It shows a rather broad pattern indicating some off-equatorial connection to the SST. This is in contrast to the interannual (ENSO) Niño4 SST mode (Figure 2b) for which the overturning regression pattern is limited to about 5^o latitude (not shown). This indicates that the STC needs more time to spin up than the TC. Figure 6 also suggests an influence from both hemispheric cells. We note that for the southern cell the mean over-

turning is negative, i.e. positive anomalies correspond to a weakening of the cell. The slightly weaker values for the northern cell might be partly due to the fact that the northern cell is weaker in the mean (25 Sv compared to 40 Sv for the southern cell, 1 Sv = 10^6 m^3s^{-1}). The weaker strength of the northern cell is due to the potential vorticity barrier associated with the Intertropical Convergence Zone (ITCZ), which prevents the subducted water to flow to the equator (*Lu and McCreary (1995), Johnson and McPhaden (1999)*). It follows from the regression pattern that a change of about 0.2 ^oC (standard deviation of the decadal Niño4 SST) goes along with a change of the cells by about 15 -20%.

To further investigate the dynamics of the decadal tropical SST variability we regress various atmospheric and oceanic fields from the NCEP forced ocean model integration onto the decadal mode timeseries (Figure 2a). The regression patterns are shown in Figure 7. A warming (cooling) in the Niño4 region goes along with a weakening (strengthening) of the trade winds over nearly the whole Tropical Pacific domain (vectors in Figure 7a). The changes are of the order of 0.01 to 0.02 Nm^{-2} per one standard deviation change in the decadal Niño4 SSTA. In the following, all described changes in the atmospheric and oceanic fields are per standard deviation change of the decadal SSTA index, even if this is not stated explicitly. Furthermore, only the warming case is described.

Weaker trade winds will lead to a reduced Ekman transport divergence at the equator in the ocean which will in turn decrease the equatorial upwelling (Figure 7b). The strongest vertical velocity changes occur in the central Pacific, where the wind stress changes are largest. In the Niño4 region, a reduction of up to 50 cm day^{-1} or about 25% of the mean upwelling is simulated. This is consistent with the study of *McPhaden and Zhang (2002)* who describe a strong decrease in the upwelling from the 1970s to the 1990s. A weakening in the trade winds will not only affect the vertical velocity at the equator, but will also weaken the wind-driven horizontal circulation. Figure 7d (vectors) shows a weakening of the South and North Equatorial Currents (SEC, NEC) of the order of 10 cm s^{-1}. Close to the equator, relatively strong meridional velocity anomalies are simulated, which reflect the weaker Ekman divergence during anomalously warm Niño4 SST. If one considers the mean horizontal temperature gradients in the Tropical Pacific, the current anomalies will advect water from the warm pool area zonally towards the east and also meridionally into the equatorial cold tongue. The horizontal temperature advection by the anomalous currents (shown by colour in Figure 7d) is determined from $-u'd\overline{T}/dx$ $-v'd\overline{T}/dy$, where the horizontal current anomalies are taken from the corresponding regression pattern (vectors in Figure 7d), and the mean temperature gradients from the observed SST data. This

horizontal advection contribution of the anomalous currents exhibits the strongest warming tendency in the region of the SEC. Splitting the advection of the mean temperature up into the zonal and meridional part (not shown) reveals the same order of magnitude for the two components in the Niño4 region (up to about $3x10^{-8}$ Ks^{-1}). For comparison, we calculate an estimate of the vertical advection by the anomalous vertical velocity according to $-w'_{65m}\,(T_{surface} - T_{90m})/90m$. At model level 65m, the upwelling reaches its maximum, but values of about 25 cm day^{-1} are simulated down to a depth of 90 meter. We estimate from the Levitus data the vertical temperature gradient to be 1 to 1.5 Kelvin over the upper 90 meter in the warm pool area, which gives (taking w'_{65m} = 25 cm day^{-1}) a value of about $4x10^{-8}$ Ks^{-1}. This value is quite similar to the estimate of the horizontal advection of the mean temperature by the anomalous horizontal currents in the Niño4 area.

The subsurface circulation weakens also during periods of anomalously warm Niño4 SST (Figure 7f). The Equatorial Undercurrent (EUC) is reduced by the order of 10 cm s^{-1}. Shown are the horizontal current anomalies at 150 meter depth, i.e. the core depth of the EUC. *Goes and Wainer (2003)* found in an NCEP forced ocean general circulation model similar reductions for the Atlantic Ocean. The EUC and SEC transports are decreased (increased) for an anomalously warm (cool) equatorial Atlantic SST. It may be noteworthy that the western boundary currents do not show a weakening during phases of anomalously warm Niño4 SST. This is consistent with *Lee and Fukumori (2003)* who describe an anticorrelation between the variations of the boundary currents and those of the interior pycnocline transport.

The surface heatflux can change the sea surface temperature in addition to the ocean dynamics. Figure 7e suggests a damping effect of the heatflux onto the SST over most of the equatorial Pacific. In the northern hemispheric part of the Niño4 region, however, the heatflux is contributing to the warming. The wind stress curl anomalies are also shown in Figure 7a (colour-shaded). A wind stress curl anomaly favouring Ekman upwelling ($w_e \sim curl\tau/f$) is simulated between about 10^o and 15^o latitude in both hemispheres during phases of anomalously warm Niño4 SST. In the southwest, the negative anomalies are due to a shift in the South Pacific Convergence Zone (SPCZ), as is clearly seen in the regression pattern for the precipitation (not shown). The effect of the off-equatorial wind stress curl anomalies is also visible in the vertical velocity (Figure 7b) and the depth of the thermocline (Figure 7c) and might contribute to the spin-down of the STCs. *Merryfield and Boer (2004, submitted)* suggest a controlling of the pycnocline transport changes due to the wind stress curl. Apart from the weakening of the off-equatorial downwelling, the shoaling of the thermocline in the west will decrease the zonal slope of the

thermocline, which itself might reduce the equatorward flow within the thermocline. Timeseries of the tilt of the thermocline at about 10^o latitude show a decreasing trend consistent with the decreasing strength of the STCs. Correlation coefficients between the anomalous thermocline depth and the STC strength at 10^o latitude as well as between the anomalous wind stress curl and the STC strength amount to about 0.7 for the Northern and to about 0.6 for the Southern Hemisphere.

The relationship between the tropical SST and the STC strength might give rise to some predictability at decadal timescales. In Figure 8, the potential predictability (interannual variance / decadal variance) of the observed SST in the Tropical Pacific is shown. While the potential predictability is close to zero in the typical ENSO region, the eastern and central equatorial Pacific, it is significant in some parts of the western equatorial Pacific and off the equator. These are basically the regions, in which the decadal mode explains most of the variance (Figure 4a). Furthermore, classical predictability studies with a CGCM, in which our ocean model is used as the ocean component, confirm the results of our potential predictability analysis and show predictive skill in exactly the same regions (*Pohlmann et al. (2004, submitted)*).

5. Simulations with a coupled general circulation model

We now turn to the decadal variability in the Tropical Pacific as simulated by the coupled ocean-atmosphere general circulation model ECHAM4/OPYC in a 300 year long control integration with constant greenhouse gas concentrations. Figure 9 shows the low-pass filtered (applying a 5-year running mean) model timeseries of the Niño4 SSTA and the maximum STC strength derived from overturning streamfunction data with a 5-year running mean applied. The level of the simulated SST variability is of the order of the observed one (Figure 1). However, no strong trend is found in the control integration with the coupled model. The STC fluctuations are comparable to those from the NCEP forced ocean model simulation, in the following denoted as MPI-OM1, before and after 1975. However, a change of the STC strength like the one which occured in the mid-seventies is not found in the coupled model integration. This is in accord with *Merryfield and Boer (2004, submitted)* who also found less pycnocline transport variability in their coupled control run than *McPhaden and Zhang (2002)* estimated from hydrographic observations. It should be mentioned, however, that the mean strength of the cells is weaker in ECHAM4/OPYC than in MPI-OM1 (30Sv compared to 40Sv for the southern and 11Sv compared to 25Sv for the northern cell).

The low-pass filtered Niño4 and STC timeseries are anticorrelated with a correlation coeffi-

cient of -0.7. The same correlation is found for the observed decadal Niño4 SSTA and the STC strength anomalies from MPI-OM1. However, in ECHAM4/OPYC the maximum correlation is found at lag zero. This lag is influenced from both hemispheric cells. While the northern cell is leading the SST by about 6 month, no such lag is found for the southern cell. The correlation pattern between the cell strength index and the SST (not shown) shows a horseshoe-like structure with maximum correlation in the western equatorial Pacific and off the equator also for the coupled model, resembling that shown in Figure 4a.

As for MPI-OM1, the cell strength shown in Figure 9 will mainly represent the equatorial part, the TCs. Figure 10 shows the cross-correlation between the low-pass filtered Niño4 SSTA and the strength of the STC at 10^{o} latitude. The strongest (anti-) correlation amounts to about -0.45, which is weaker than for MPI-OM1, but still statistically significant at the 95% level (threshold value -0.21). The fact that the cells are weaker compared to MPI-OM1 might contribute to the lower correlation, although the correlation is similar for the near-equatorial overturning. The regression pattern of the meridional overturning onto the low-pass filtered Niño4 SSTA (not shown) also suggests a weaker influence from off-equatorial regions than in MPI-OM1. As in MPI-OM1, the strongest (anti-) correlation is found if the cell strength at 10^{o} latitude is leading the Niño4 SSTA by about one year. Thus, the CGCM integration supports our notion that the low-frequency variability in the STCs is important in driving western equatorial and off-equatorial SST anomalies. At 10^{o} latitude, the lag is similar for both hemispheres. A secondary extreme is found in the cross-correlation function, when the SSTA is leading the cell strength. This suggests that changes in the SST might contribute (via changes in the trade winds) to changes in the cell strength. Such a feedback is not seen in the uncoupled OGCM run (Figure 5b). It is found, however, if the MPI-OM1 model is coupled to the atmosphere model ECHAM5 (not shown).

We performed again a SSA of the monthly Niño4 SSTA and consider the two leading modes. In contrast to the observed SST, the leading SSA mode of the coupled model has an interannual timescale representing the ENSO mode, while the second most energetic mode is the decadal mode. This seems to be due to the fact that the coupled model simulates an El Niño period of only two years and slightly too strong ENSO variability. If the SSA is calculated from annual values rather than from monthly values so that the ENSO frequency is not fully resolved, the decadal mode turns out to be the leading one. We regress various atmospheric and oceanic fields onto the decadal Niño4 SSTA mode. Overall, the regression patterns derived from the CGCM (Figure 11) are similar to the ones derived from MPI-OM1 (Figure 7). If one takes into account

the different standard deviations of the decadal Niño4 SSTA modes (0.13^{o}C for the CGCM compared to 0.21^{o}C for the observed one), the values have the same order of magnitude. We note that the scale in Figure 11 is different to that in Figure 7 and that in both cases the regression coefficients are expressed per standard deviation in the SSTA.

In ECHAM4/OPYC, the weakening of the surface wind stress (vectors in Figure 11a) during an increase in the Niño4 SST is confined to the western part of the basin. This is also the case, if the SST index is averaged over the entire width of the Pacific. Accordingly, the maximum equatorial upwelling anomalies are simulated in the west (Figure 11b) where the mean upwelling is small. The signal in the wind stress curl (colour-shaded in Figure 7a) is also confined to the western part of the basin. As in MPI-OM1, the anomalies in the southwest Tropical Pacific are due to a shift in the SPCZ as seen again in the regression pattern for the precipitation (not shown). The changes in the depth of the thermocline in the western and central part are much weaker than in MPI-OM1, but the spatial structure is similar with a shoaling in the west and a deepening in the east. In MPI-OM1, the dominating change is the decreasing trend in the slope of the thermocline. Such a signal is not found in the ECHAM4/OPYC control run. The deepening of the thermocline in the east exists also in MPI-OM1. It is not seen in Figure 7, because the depth of the thermocline has been determined by the depth of the 20^{o}C isotherm which is partly outcropping in the east in MPI-OM1, so that no regression coefficients could be calculated.

Considering the horizontal surface circulation (Figure 7d) the weakening of the SEC in the east is quite strong. This is at least partly due to the fact that the mean SEC is relatively strong in the east in this model (70 cm s^{-1} compared to 50 cm s^{-1} in MPI-OM1). In the west, a strengthening of the North Equatorial Countercurrent (NECC) during a warming of the Niño4 SST is simulated by the coupled model. Since anomalously warm SST goes along with weaker cells, this might reflect the fact that the ITCZ together with the NECC weaken the northern cell by providing a potential vorticity barrier. At the equator, a wind driven jet is found in the west. Due to this jet and the strengthened NECC the horizontal advection (colour-shaded in Figure 7d) contributes, in contrast to MPI-OM1, to a warming in the west north of the equator. This difference might be due to the trend. If the observed SSTs are detrended prior to the regression analysis, the regression pattern from MPI-OM1 shows a wind driven jet too. Considering the subsurface circulation (Figure 7f), it should be mentioned that the EUC is reduced over the whole width of the basin. Since the EUC core rises towards the east, the changes in the east are visible in the regression patterns for model levels 50 and 100 meter (not shown). The surface

heatflux acts as a damping at the equator, in agreement with MPI-OM1. It also contributes to the warming in the north western equatorial Pacific, although this contribution is confined to the region west of of the dateline.

Apart from the control integration, a 240 year long scenario integration is available from the ECHAM4/OPYC model to study the sensitivity of the STCs to greenhouse warming. This integration was analyzed, for instance, by *Timmermann et al. (1999)* who investigated the ENSO response to greenhouse warming. The integration is forced by observed greenhouse concentrations from 1860 to present and the concentrations follow the IPCC 1992a scenario until 2100. Figure 12a shows an index of the strength of the cells for the near-equatorial part. As for the control integration, the index has been determined from overturning data with a 5-year running mean applied. The strength of the equatorial cells is obviously increasing under greenhouse conditions. Such a trend is not seen in the control integration (blue curve in figure 9). *Merryfield and Boer (2004, submitted)* found a decrease of the pycnocline transport at 10^o latitude under global warming conditions. Therefore we determine the STC strength at different latitudes. The coupled model simulates indeed a decreasing trend poleward of 10^o latitude. This is seen clearly at 15^o latitude (Figure 12b), where the transport weakens considerably during the 21st century. Thus, the CGCM simulates a quite complex global warming response of the tropical circulation. While the shallow equatorial cells intensify, the off-equatorial and deeper components spin down (Figure 13). The latter is consistent with the uncoupled OGCM simulation discussed above. A more detailed discussion of the results of the scenario integration is beyond the scope of this paper.

6. Conclusions

In this paper we have investigated the origin of the decadal SST variability in the Tropical Pacific. The leading mode in the western equatorial Pacific is a decadal mode. Its spatial structure is El Niño-like, but it explains most variance in the western equatorial Pacific and off the equator. The warming trend observed during the most recent decades projects onto the decadal mode. Our analysis suggests that the decadal variability (including the trend) is closely connected to the variability of the wind driven subtropical-tropical cells (STCs). Changes in strength of the STCs lead the changes in the SST. The lag becomes larger with increasing latitude, which indicates that the subtropical cells adjust slower than the equatorial cells. Different processes play important roles in the connection between STC and SST, including horizontal and vertical advection of the mean temperature by anomalous currents. The surface heat flux acts in most

regions as a damping. Thus, it is the ocean dynamics that drive the decadal SST variability in large regions of the Tropical Pacific. In the eastern equatorial Pacific, the STC variability does not explain much of the SST variability. The SST in this region is mainly determined by the depth of the thermocline. In the NCEP forced ocean model simulation as well as in the coupled model simulation, correlation coefficients between the SST anomalies and anomalies of the depth of the thermocline are of the order of 0.8 to 0.9 for interannual as well as decadal timescales.

The results of the coupled control run suggests the existence of a coupled feedback loop between the SST and the STCs. One possible feedback hypothesis is described in the following. We start the loop with anomalously strong (weak) STCs. These in turn will drive colder (warmer) SSTs in the equatorial Pacific that are La Niña- (El Niño)-like. The SST anomalies will force characteristic off-equatorial wind stress curl anomalies, eventually weakening (strengthening) the STCs, which completes the phase reversal. Further work is needed, however, to prove this hypothesis. The results of a greenhouse warming integration with the same coupled model reveal a strengthening of the equatorial components and weakening of the off-equatorial components of the STC.

Acknowledgements

We thank Dr. Noel Keenlyside for helpful discussion during all stages of the work and Monika Esch for helping with the OPYC data.This work was supported by the Ocean-CLIVAR programme of the BMBF and by the ENSEMBLES project of the European Union. The numerical model integrations were performed at the Deutsches Klimarechenzentrum.

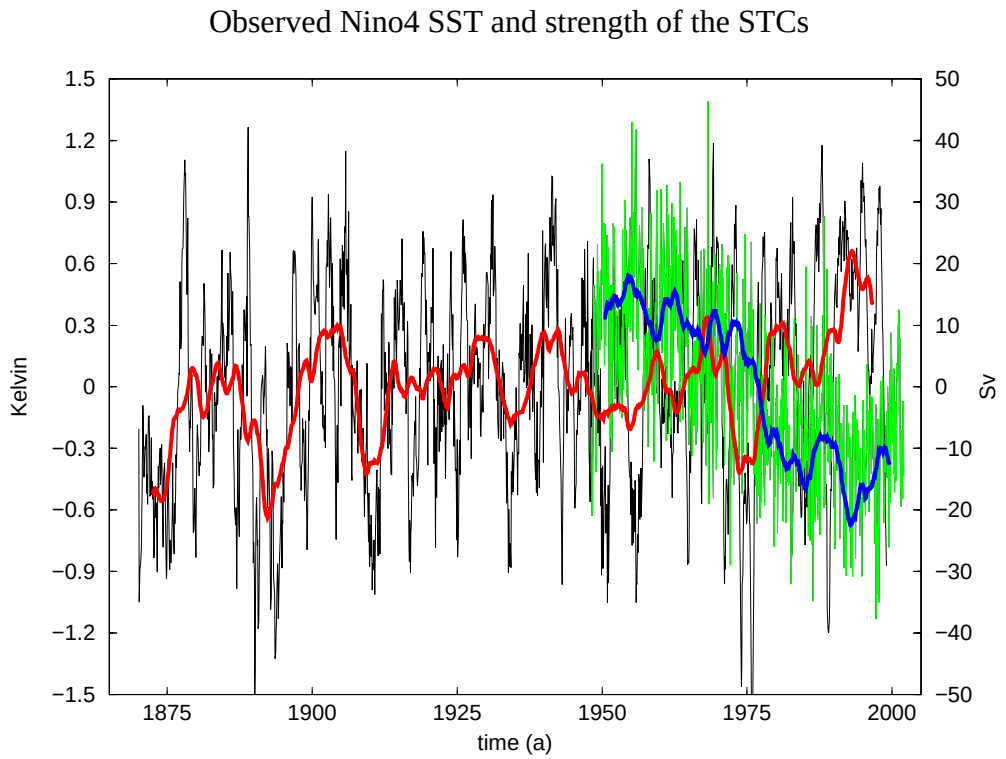

***Figure 1**: Timeseries of the observed Niño4 SST anomalies and the anomalous strength of the subtropical-tropical cells (STCs) taken from an NCEP forced ocean model. For definition of the cell strength see text. Shown are monthly values with the annual cycle removed (black for SST, green for STC) and five year running mean (red for SST, blue for STC).*

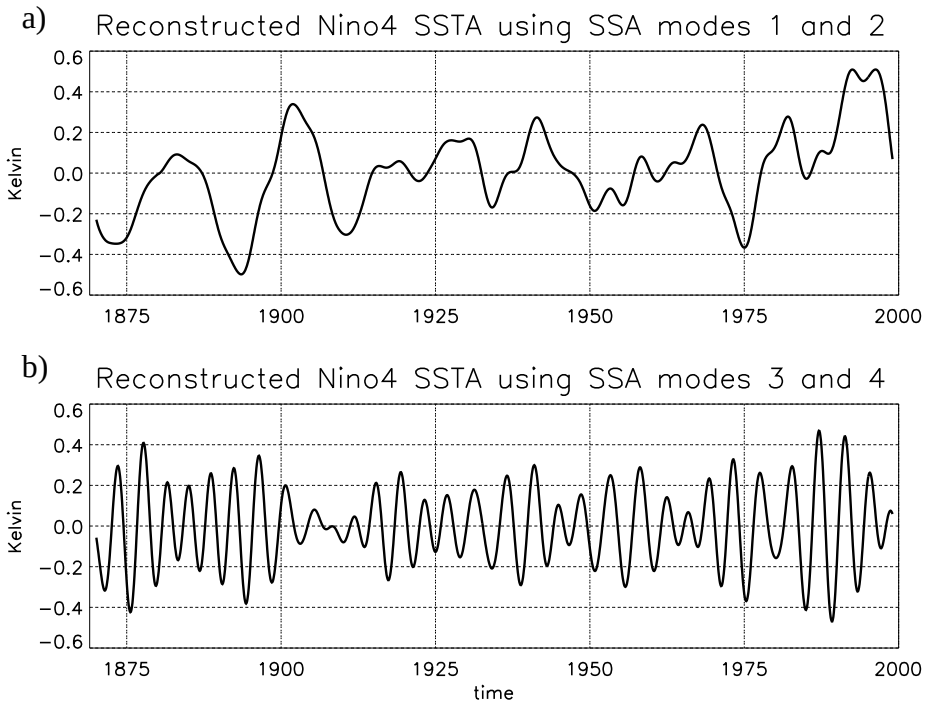

***Figure 2**: Reconstruction of the monthly observed Niño4 SST anomalies from singular spectrum analysis using (a) mode 1 and 2 and (b) mode 3 and 4.*

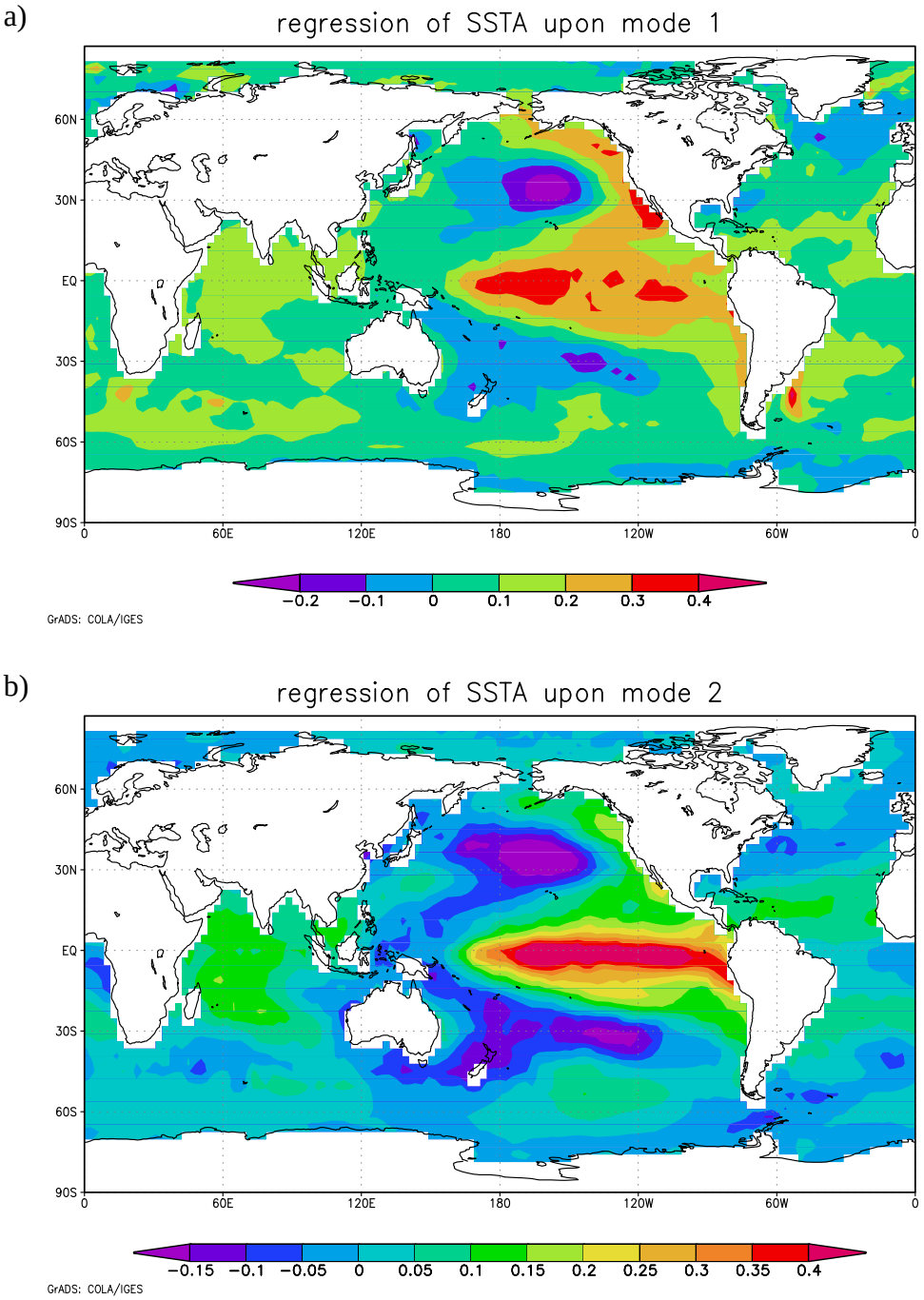

***Figure 3**: Regression of the monthly global observed SST onto the Niño4 modes shown in figure 2: (a) decadal mode, (b) interannual mode. Unit is Kelvin per standard deviation Niño4 SST. The standard deviation is 0.21K for the decadal and 0.18K for the interannual mode.*

a)

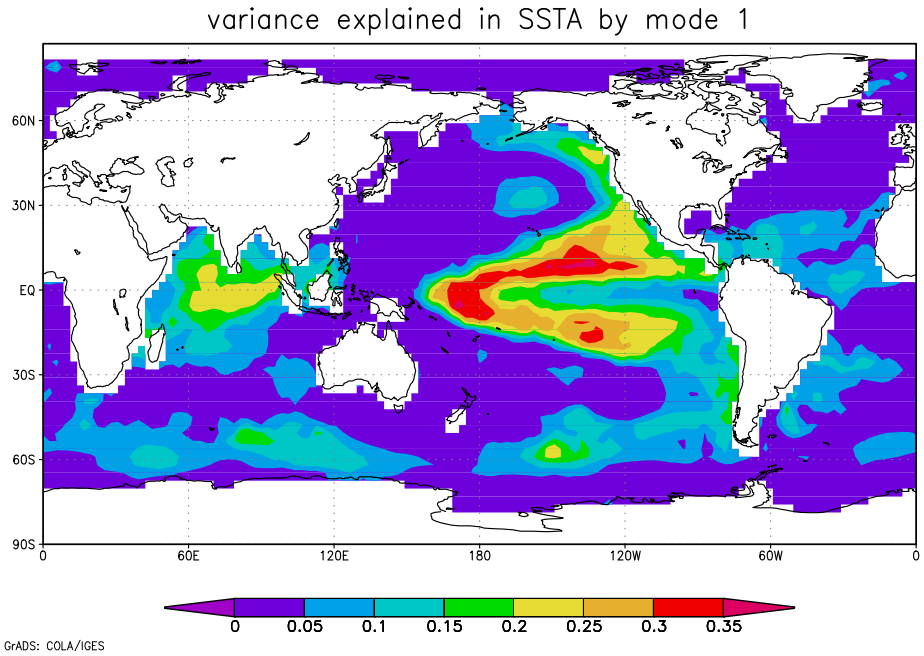

b)

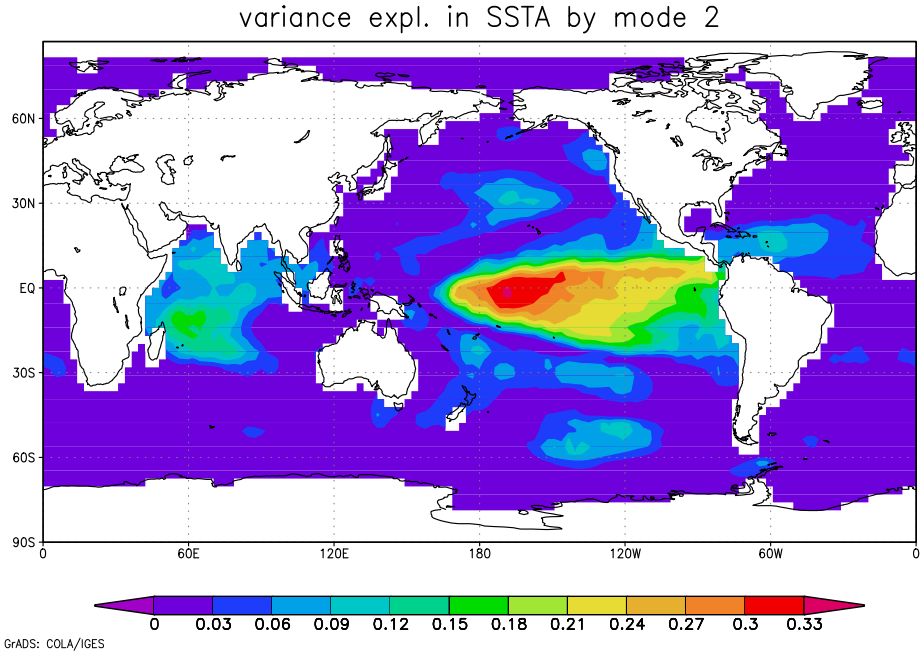

***Figure 4**: Explained variance of the regression pattern shown in figure 3: (a) for the regression onto the decadal mode, (b) for the regression onto the interannual mode.*

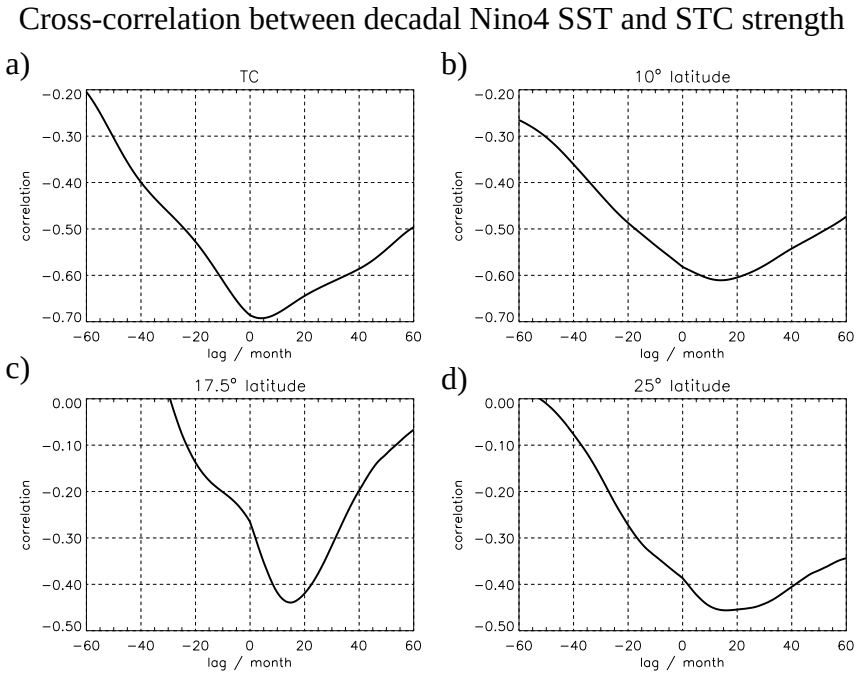

***Figure 5**: Cross-correlation function between the decadal observed Niño4 SST (red curve in figure 1, years 1948-1998) and the STC strength at different latitudes taken from an NCEP forced ocean model. For definition of the cell strength see text. The 95% significance level according to a t-test is -0.44. A positive (negative) lag indicates that the Niño4 SST is lagging (leading).*

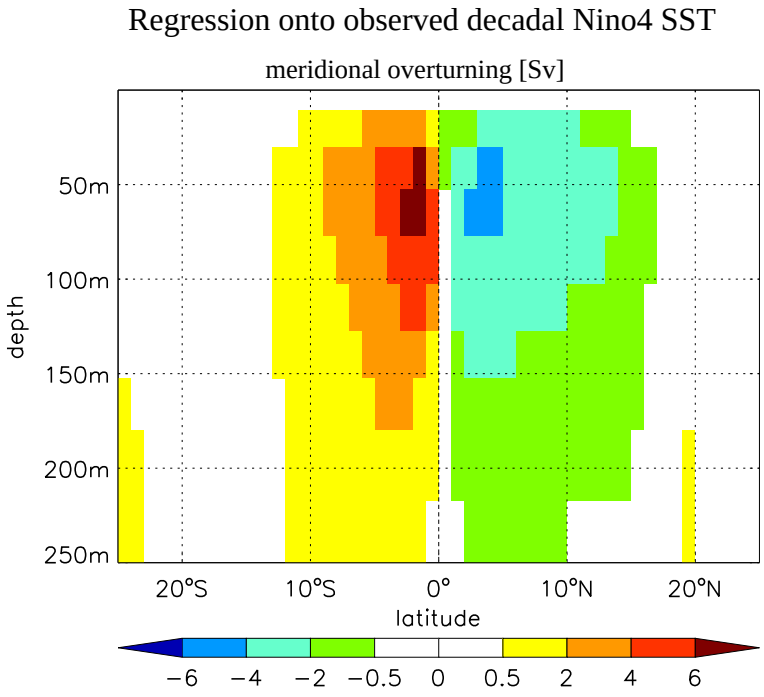

***Figure 6**: Regression of the monthly Pacific overturning (with annual cycle removed) onto the observed decadal Niño4 SST mode from figure 2a. The overturning is taken from an NCEP forced ocean model. Unit is Sverdrup (1 Sv = 10^6 m^3/s) per standard deviation SST (0.21K). Note that for the southern cell the overturning is negative.*

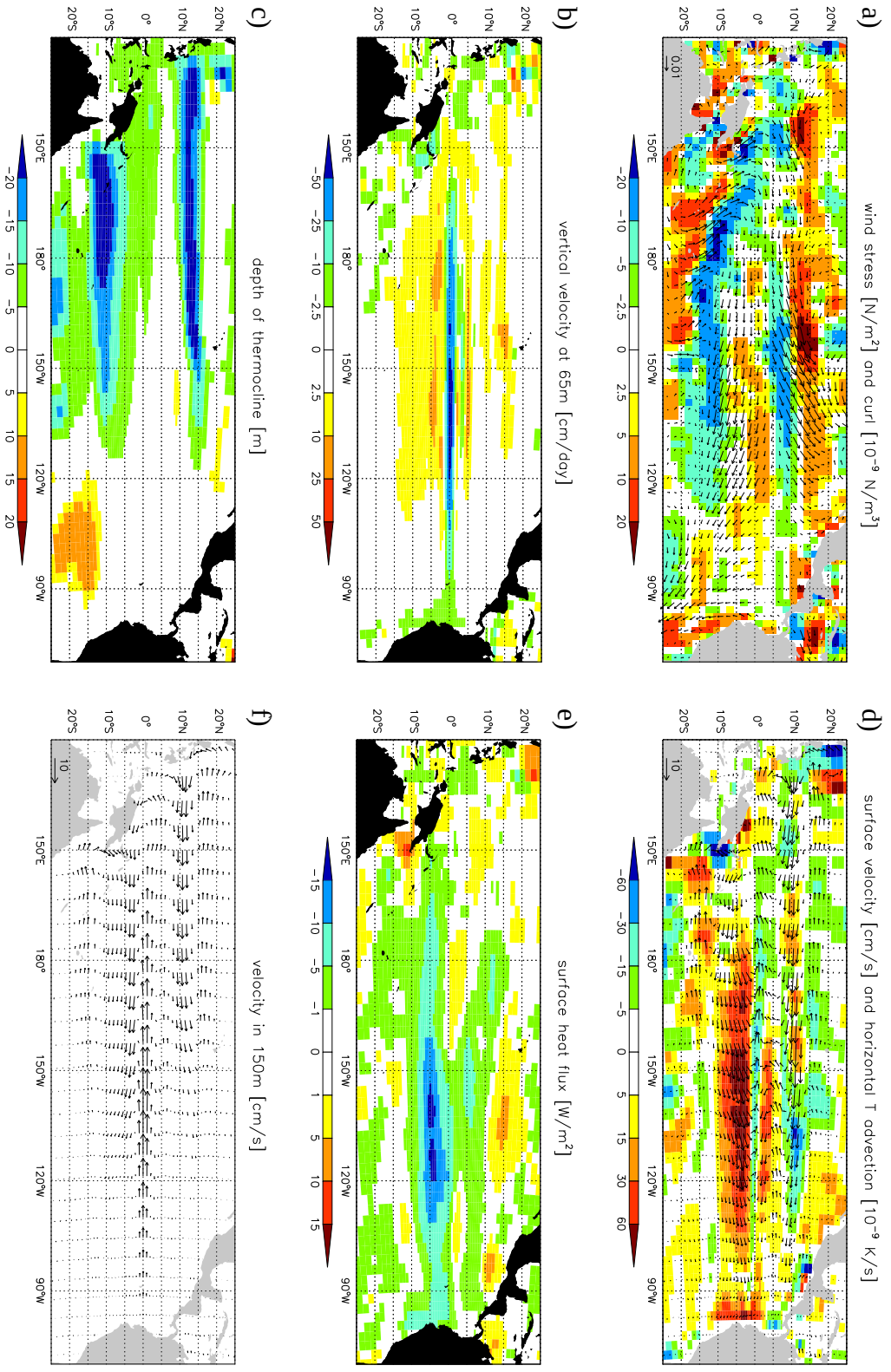

***Figure 7**: Regression of various atmospheric and oceanic fields (from NCEP re-analysis and NCEP forced ocean model) onto the observed decadal Niño4 SST mode from figure 2a. The fields are monthly values with the annual cycle removed. All values are per standard deviation SST (0.21K). (a) windstress (vectors, in N/m^2) and wind stress curl (contours, in 10^{-9} N/m^3), (b) vertical velocity at model level 65 meter (in cm/day), (c) depth of the thermocline (in m), (d) horizontal velocity at the surface (in cm/s) and horizontal temperature advection (in 10^{-9} K/s), (e) net surface heat flux (in W/m^2), (f) horizontal velocity at model level 150 meter (in cm/s).*

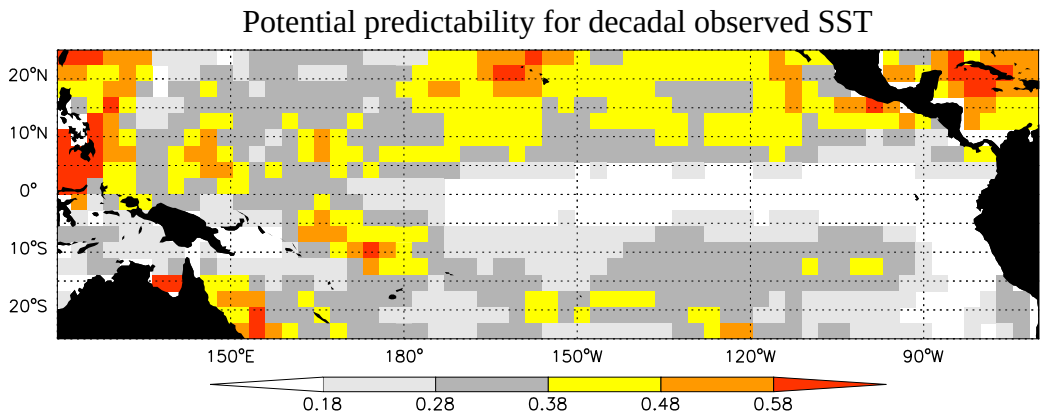

***Figure 8**: Potential predictability for decadal observed SST defined by variance of annual values divided by variance of 10 year means. Significant values according to an F-test are shown in color.*

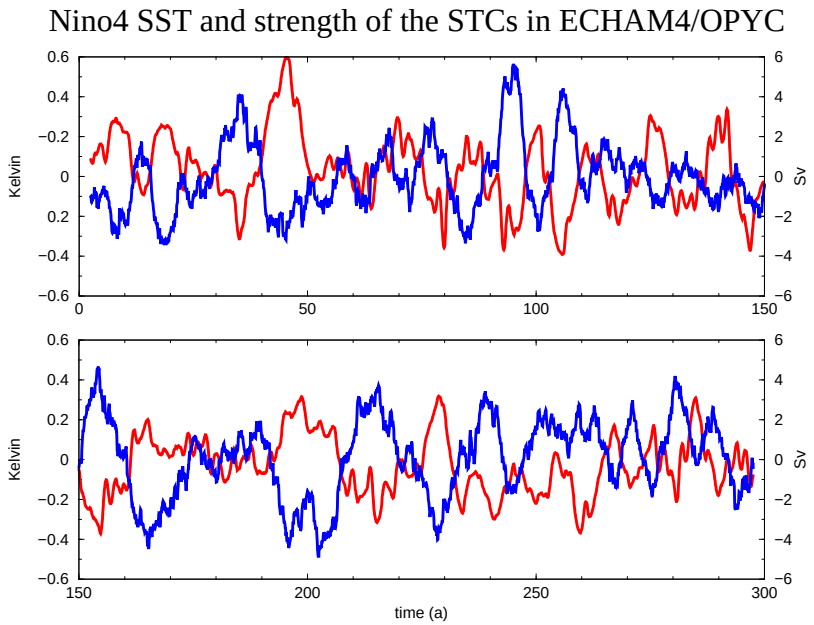

***Figure 9**: Timeseries of the Niño4 SST anomalies and the anomalous strength of the STCs from the ECHAM4/OPYC model. For definition of the cell strength see text. Shown are only five year running mean values (red for SST, blue for STC).*

Cross-correlation between decdal Nino4 SST and STC strength

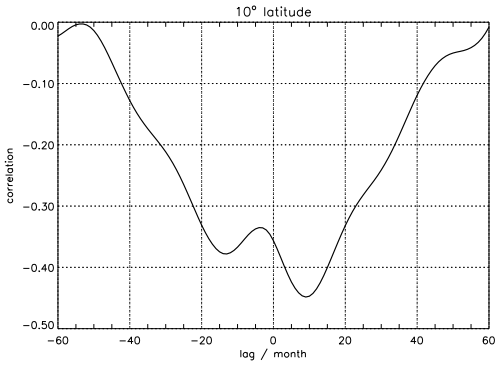

***Figure 10**: Cross-correlation function between the decadal Niño4 SST (red curve in figure 9) and the STC strength at 10^o latitude from the ECHAM4/OPYC model. For definition of the cell strength see text. The 95% significance level according to a t-test is -0.21. A positive (negative) lag indicates that the Niño4 SST is lagging (leading).*

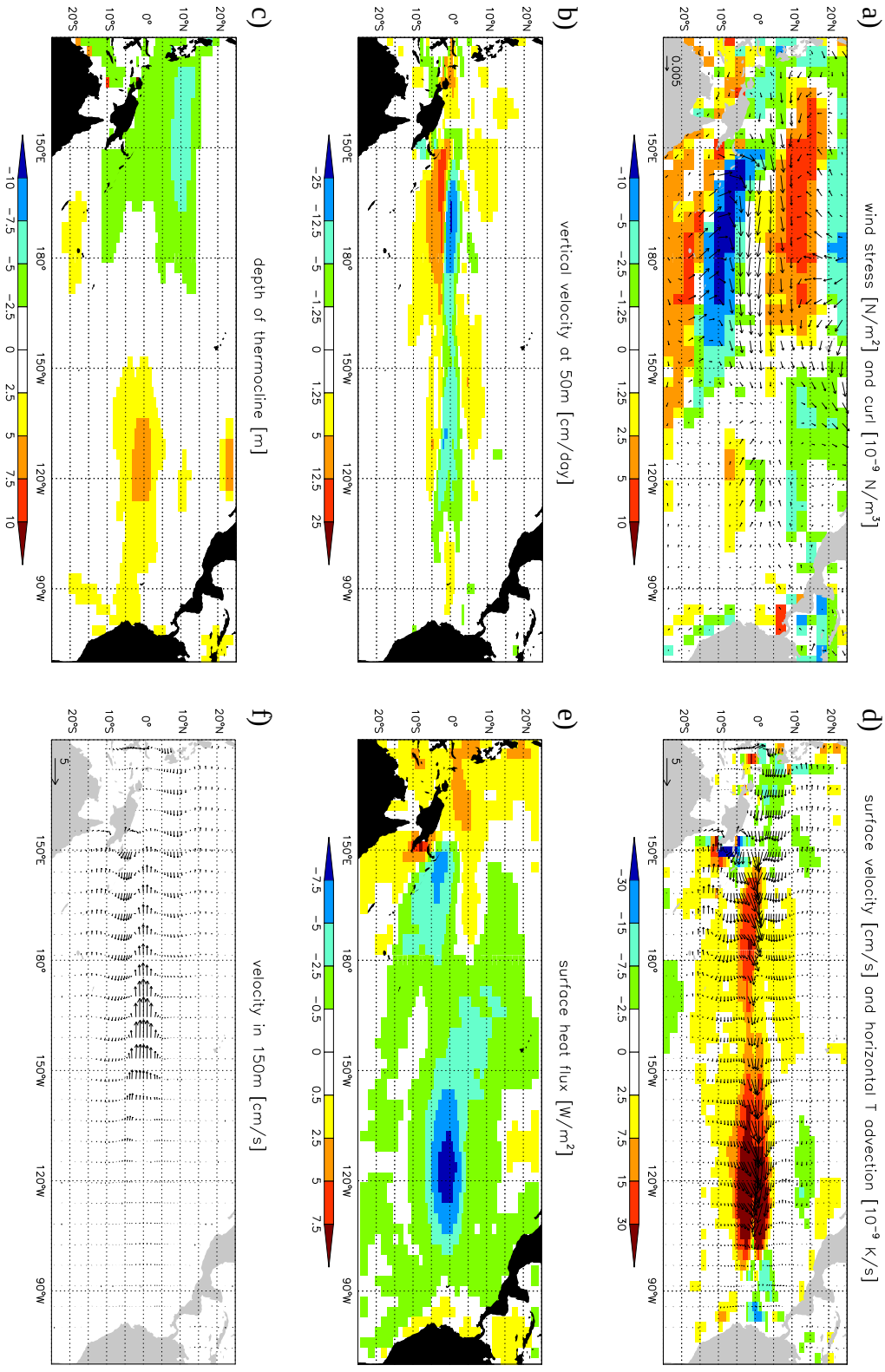

Figure 11:*Regression of various atmospheric and oceanic fields onto the decadal Niño4 SST mode from a singular spectrum analysis for the ECHAM4/OPYC model. The fields are monthly values with the annual cycle removed. All values are per standard deviation SST (0.13K). (a) windstress (vectors, in N/m^2) and wind stress curl (contours, in 10^{-9} N/m^3), (b) vertical velocity at model level 65 meter (in cm/day), (c) depth of the thermocline (in m), (d) horizontal velocity at the surface (in cm/s) and horizontal temperature advection (in 10^{-9} K/s), (e) net surface heat flux (in W/m^2), (f) horizontal velocity at model level 150 meter (in cm/s).*

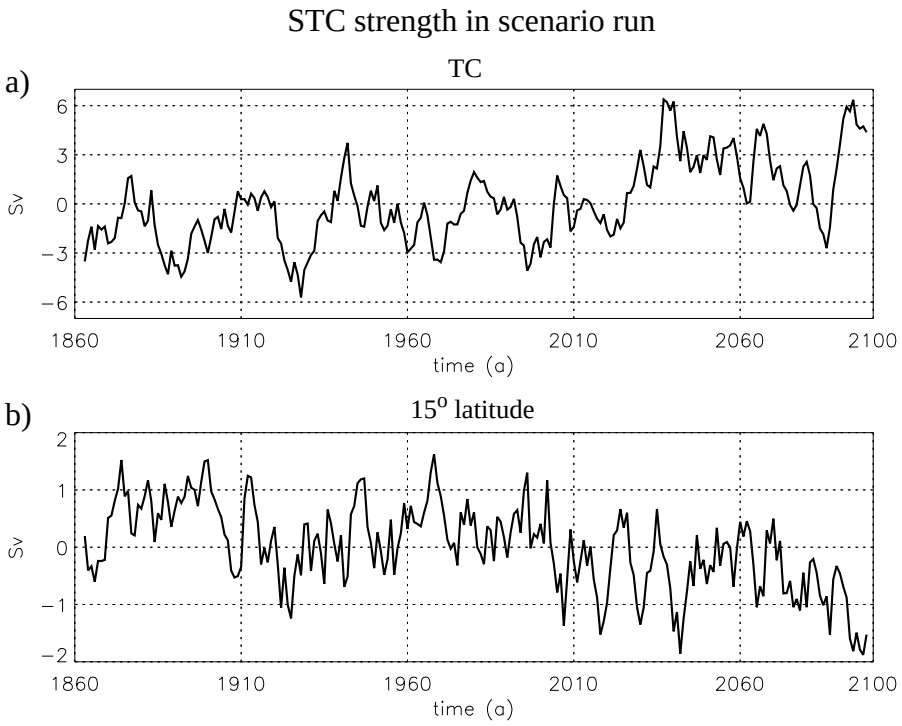

***Figure 12**: Timeseries of the anomalous strength of the STCs from a scenario run of the ECHAM4/ OPYC model. For definition of the cell strength see text. Shown are only five year running mean values, (a) equator near part (maximum strength) and (b) at 15° latitude.*

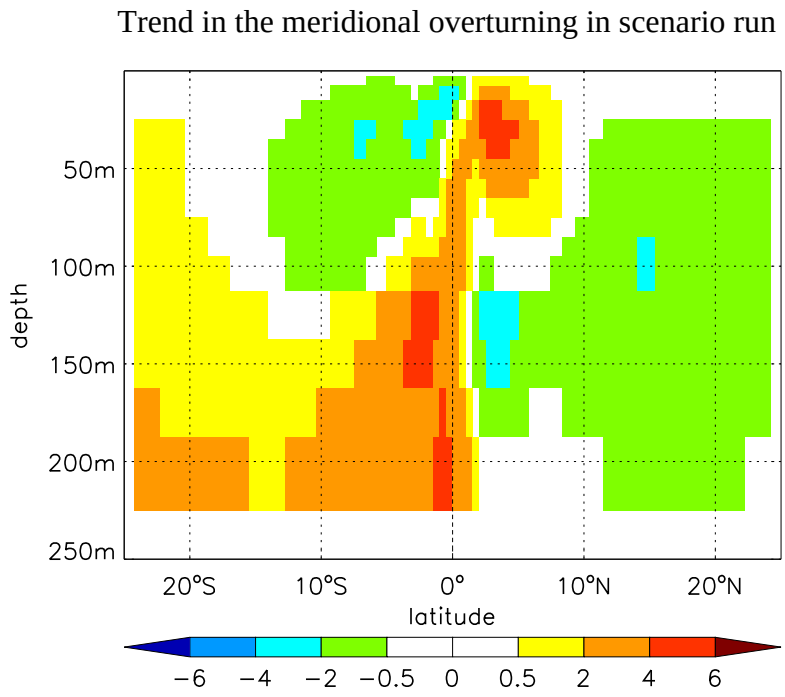

***Figure 13**: Trend in the meridional overturning from a scenario run of the ECHAM4/OPYC model. Unit is Sv over the last 110 years of the run (1990-2100). Note that for the southern hemispheric cell the mean is negative, i.e. negative (positive) values correspond to a strengthening (weakening) of the overturning.*

References

Boccaletti, G., R. Pacanowski and S. Philander, 2003: A diabatic mechanism for decadal variability in the tropics. *Journal of Climate*, submitted

Giese, B., S. Urizar and N. Fuckar, 2002: Southern hemisphere origins of the 1976 climate shift. *Geophysical Research Letters*, **29**, 1014

Goes, M. and I. Wainer, 2003: Equatorial currents transport changes for extreme warm and cold events in the Atlantic Ocean. *Geophysical Research Letters*, **30**, Cli-6

Gu, D. and S. Philander, 1997: Interdecadal climate fluctuations that depend on exchanges between the tropics and extratropics. *Science*, **275**, 805-807.

Hazeleger, W., M. Visbeck, M. Cane, A. Karspeck and N. Naik, 2001: Decadal upper ocean temperature variability in the tropical Pacific. *Journal of Geophysical Research*, **106**, 8971-8988.

Hazeleger, W., P. DeVries and Y. Friocourt, 2003: Sources of the Equatorial Undercurrent in the Atlantic in a high-resolution ocean model. *Journal of Physical Oceanography*, **33**, 677-693.

IPCC, Climate change, 1995: The science of climate change, edited by J. Houghton, L. Meira Filho, B. Callendar, N. Harris, A. Kattenberg and K. Maskell. Cambridge University Press, New York, 572pp., 1996

Johnson, G. and M. McPhaden, 1999: Interior pycnocline flow from the subtropical to the equatorial Pacific Ocean. *Journal of Physical Oceanography*, **29**, 3073-3089.

Johnson, G., 2001: The Pacific Ocean subtropical cell surface limb. *Geophysical Research Letters*, **28**, 1771-1774.

Kleeman, R., J. McCreary and B. Klinger, 1999: A mechanism for generating ENSO decadal variability. *Geophysical Research Letters*, **26**, 1743-1746.

Klinger, B., J. McCreary and R. Kleeman, 2002: The relationship between oscillating subtropical wind stress and equatorial temperature. *Journal of Physical Oceanography*, **32**, 1507-1521.

Latif, M., R. Kleeman and C. Eckert, 1997: Greenhouse warming, decadal variability or El Niño: An attempt to understand the anomalous 1990‘s. *Journal of Climate*, **10**, 2221-2239.

Latif, M., E. Roeckner, M. Botzet, M. Esch, H. Haak, S. Hagemann, J. Jungclaus, S. Legutke, S. Marsland, U. Mikolajewicz and J. Mitchell, 2004: Reconstructing, monitoring and predicting decadal-scale changes in the North Atlantic thermohaline circulation with sea surface temperature. *Journal of Climate*, in press

Lee, T. and I. Fukumori, 2003: Interannual-to-decadal variations of tropical-subtropical exchange in the Pacific Ocean: Boundary versus interior pycnocline transports. *Journal of Climate*, **16**, 4022-4042.

Liu, Z., 1994: A simple model of the mass exchange between the subtropical and tropical ocean. *Journal of Physical Oceanography*, **24**, 1153-1165.

Liu, Z., 1998: The role of ocean in the response of tropical climatology to global warming: The west-east SST contrast. *Journal of Climate*, **11**, 864-875.

Lu, P. and J. McCreary, 1995: Influence of the ITCZ on the flow of thermocline water from the subtropical to the equatorial Pacific Ocean. *Journal of Physical Oceanography*, **25**, 3076-3088.

Lu, P., J. McCreary and B. Klinger, 1998: Meridional circulation cells and the source waters of the Pacific Equatorial Undercurrent. *Journal of Physical Oceanography*, **28**, 62-84.

Marsland, S., H. Haak, J. Jungclaus, M. Latif and F. Roeske, 2003: The Max-Planck-Institute global ocean/sea ice model with orthogonal curvilinear coordinates. *Ocean Modelling*, **5**, 91-127.

McCreary, J. and P. Lu, 1994: Interaction between the subtropical and equatorial ocean circu-

lations: the subtropical cell. *Journal of Physical Oceanography*, **24**, 466-497.
McPhaden, M. and D. Zhang, 2002: Slowdown of the meridional overturning circulation in the upper Pacific Ocean. *Nature*, **415**, 603-608.
Merryfield, W. and G. Boer, 2004: Variability of upper Pacific Ocean overturning in a coupled climate model. *Journal of Climate*, submitted
Nonaka, M., S.-P. Xie and J. McCreary, 2002: Decadal variations in the subtropical cells and equatorial Pacific SST. *Geophysical Research Letters*, **29**, 20
Oberhuber, J., 1993: Simulation of the Atlantic circulation with a coupled sea ice - mixed layer - isopycnal general circulation model. Part I: Model description. *Journal of Physical Oceanography*, **23**, 808-829.
Pohlmann, H., M. Botzet, M. Latif, A. Roesch, M. Wild and P. Tschuck, 2004: Estimating the long-term predictability potential of a coupled AOGCM. *Journal of Climate*, submitted
Rayner, N., D. Parker, E. Horton, C. Folland, L. Alexander, D. Rowell, E. Kent and A. Kaplan, 2003: Global analyses of SST, sea ice and night marine air temperature since the late nineteenth century. *Journal of Geophysical Research*, **108**, 4407
Roeckner, E., K. Arpe, L. Bengtsson, M. Christoph, M. Claussen, L. Duemenil, M. Esch, M. Giorgetta, U. Schlese and U. Schulzweida, 1996: The atmospheric general circulation model ECHAM-4: Model description and simulation of present-day climate. Report 218, Max-Planck-Institut fuer Meteorologie, Hamburg, Germany
Roeckner, E., L. Bengtsson, J. Feichter, J. Lelieveld and H. Rohde, 1999: Transient climate change simulations with a coupled atmosphere-ocean GCM including the tropospheric sulfur cycle. *Journal of Climate*, **12**, 3004-3032.
Schneider, N., S. Venzke, A. Miller, D. Pierce, T. Barnett, C. Deser and M. Latif, 1999: Pacific thermocline bridge revisited. *Geophysical Research Letters*, **26**, 1329-1332.
Solomon, A., J. McCreary, R. Kleeman and B. Klinger, 2003: Interannual and decadal variability in an intermediate coupled model of the Pacific region. *Journal of Climate*, **16**, 383-405.
Timmermann, A., M. Latif, A. Bacher, J. Oberhuber and E. Roeckner, 1999: Increased El Nino frequency in a climate model forced by future greenhouse warming. *Nature*, **398**, 694-696.
Wu, R. and S.-P. Xie, 2003: On equatorial Pacific wind changes around 1977: NCEP-NCAR reanalysis versus COADS observations. *Journal of Climate*, **16**, 167-173.
Yang, H. and Z. Liu, 2003: Tropical-extratropical and inter-hemispheric climate interaction: Atmospheric bridge and oceanic tunnel. *Journal of Climate*, submitted
Zhang, R.-H., L. Rothstein and A. Busalacchi, 1998: Origin of upper-ocean warming and El Nino change on decadal scales in the tropical Pacific Ocean. *Nature*, **391**, 879-883.
Zhang, Y., J. Wallace and D. Battisti, 1997: ENSO-like interdecadal variability: 1900-93. *Journal of Climate*, **10**, 1004-1020.

MPI-Report-Reference: *Reprinted in

Report 1 - 302 Please order the reference list from MPI for Meteorology, Hamburg

Report No. 303
December 1999
The leading variability mode of the coupled troposphere-stratosphere winter circulation in different climate regimes
Judith Perlwitz, Hans-F. Graf, Reinhard Voss
* Journal of Geophysical Research, 105, 6915-6926, 2000

Report No. 304
January 2000
Generation of SST anomalies in the midlatitudes
Dietmar Dommenget, Mojib Latif
* Journal of Climate, 1999 (submitted)

Report No. 305
June 2000
Tropical Pacific/Atlantic Ocean Interactions at Multi-Decadal Time Scales
Mojib Latif
* Geophysical Research Letters, 28,3,539-542,2001

Report No. 306
June 2000
On the Interpretation of Climate Change in the Tropical Pacific
Mojib Latif
* Journal of Climate, 2000 (submitted)

Report No. 307
June 2000
Observed historical discharge data from major rivers for climate model validation
Lydia Dümenil Gates, Stefan Hagemann, Claudia Golz

Report No. 308
July 2000
Atmospheric Correction of Colour Images of Case I Waters - a Review of Case II Waters - a Review
D. Pozdnyakov, S. Bakan, H. Grassl
* Remote Sensing of Environment, 2000 (submitted)

Report No. 309
August 2000
A Cautionary Note on the Interpretation of EOFs
Dietmar Dommenget, Mojib Latif
* Journal of Climate, 2000 (submitted)

Report No. 310
September 2000
Midlatitude Forcing Mechanisms for Glacier Mass Balance Investigated Using General Circulation Models
Bernhard K. Reichert, Lennart Bengtsson, Johannes Oerlemans
* Journal of Climate, 2000 (accepted)

Report No. 311
October 2000
The impact of a downslope water-transport parameterization in a global ocean general circulation model
Stephanie Legutke, Ernst Maier-Reimer

Report No. 312
November 2000
The Hamburg Ocean-Atmosphere Parameters and Fluxes from Satellite Data (HOAPS): A Climatological Atlas of Satellite-Derived Air-Sea-Interaction Parameters over the Oceans
Hartmut Graßl, Volker Jost, Ramesh Kumar, Jörg Schulz, Peter Bauer, Peter Schlüssel

Report No. 313
December 2000
Secular trends in daily precipitation characteristics: greenhouse gas simulation with a coupled AOGCM
Vladimir Semenov, Lennart Bengtsson

Report No. 314
December 2000
Estimation of the error due to operator splitting for micro-physical-multiphase chemical systems in meso-scale air quality models
Frank Müller
* Atmospheric Environment, 2000 (submitted)

Report No. 315
January 2001
Sensitivity of global climate to the detrimental impact of smoke on rain clouds (only available as pdf-file on the web)
Hans-F. Graf, Daniel Rosenfeld, Frank J. Nober

Report No. 316
March 2001
Lake Parameterization for Climate Models
Ben-Jei Tsuang, Chia-Ying Tu, Klaus Arpe

Report No. 318
March 2001
On North Pacific Climate Variability
Mojib Latif
* Journal of Climate, 2001 (submitted)

MPI-Report-Reference: *Reprinted in

Report 1 - 302 Please order the reference list from MPI for Meteorology, Hamburg

Report No. 319
March 2001
The Madden-Julian Oscillation in the ECHAM4 / OPYC3 CGCM
Stefan Liess, Lennart Bengtsson, Klaus Arpe
* Climate Dynamics, 2001 (submitted)

Report No. 320
May 2001
Simulated Warm Polar Currents during the Middle Permian
A. M. E. Winguth, C. Heinze, J. E. Kutzbach, E. Maier-Reimer,
U. Mikolajewicz, D. Rowley, A. Rees, A. M. Ziegler
* Paleoceanography, 2001 (submitted)

Report No. 321
June 2001
Impact of the Vertical Resolution on the Transport of Passive Tracers in the ECHAM4 Model
Christine Land, Johann Feichter, Robert Sausen
* Tellus, 2001 (submitted)

Report No. 322
August 2001
Summer Session 2000
Beyond Kyoto: Achieving Sustainable Development
Edited by Hartmut Graßl and Jacques Léonardi

Report No. 323
July 2001
An atlas of surface fluxes based on the ECMWF Re-Analysis- a climatological dataset to force global ocean general circulation models
Frank Röske

Report No. 324
August 2001
Long-range transport and multimedia partitioning of semivolatile organic compounds:
A case study on two modern agrochemicals
Gerhard Lammel, Johann Feichter, Adrian Leip
* Journal of Geophysical Research-Atmospheres, 2001 (submitted)

Report No. 325
August 2001
A High Resolution AGCM Study of the El Niño Impact on the North Atlantic / European Sector
Ute Merkel, Mojib Latif
* Geophysical Research Letters, 2001 (submitted)

Report No. 326
August 2001
On dipole-like varibility in the tropical Indian Ocean
Astrid Baquero-Bernal, Mojib Latif
* Journal of Climate, 2001 (submitted)

Report No. 327
August 2001
Global ocean warming tied to anthropogenic forcing
Berhard K. Reichert, Reiner Schnur, Lennart Bengtsson
* Geophysical Research Letters, 2001 (submitted)

Report No. 328
August 2001
Natural Climate Variability as Indicated by Glaciers and Implications for Climate Change: A Modeling Study
Bernhard K. Reichert, Lennart Bengtsson, Johannes Oerlemans
* Journal of Climate, 2001 (submitted)

Report No. 329
August 2001
Vegetation Feedback on Sahelian Rainfall Variability in a Coupled Climate Land-Vegetation Model
K.-G. Schnitzler, W. Knorr, M. Latif, J.Bader, N.Zeng
Geophysical Research Letters, 2001 (submitted)

Report No. 330
August 2001
Structural Changes of Climate Variability **(only available as pdf-file on the web)**
H.-F.Graf, J. M. Castanheira
Journal of Geophysical Research -Atmospheres, 2001 (submitted)

Report No. 331
August 2001
North Pacific - North Atlantic relationships under stratospheric control? (only available as pdf-file on the web)
H.-F.Graf, J. M. Castanheira
Journal of Geophysical Research -Atmospheres, 2001 (submitted)

Report No. 332
September 2001
Using a Physical Reference Frame to study Global Circulation Variability (only available as pdf-file on the web)
H.-F.Graf, J. M. Castanheira, C.C. DaCamara, A.Rocha

MPI-Report-Reference:		*Reprinted in
Report 1 - 302	Please order the reference list from MPI for Meteorology, Hamburg	
	Journal of Atmospheric Sciences, 2001 (in press)	
Report No. 333 November 2001	**Stratospheric Response to Global Warming in the Northern Hemisphere Winter** Zeng-Zhen Hu	
Report No. 334 October 2001	**On the Role of European and Non-European Emission Sources for the Budgets of Trace Compounds over Europe** Martin G. Schultz, Johann Feichter, Stefan Bauer, Andreas Volz-Thomas	
Report No. 335 November 2001	**Slowly Degradable Organics in the Atmospheric Environment and Air-Sea Exchange** Gerhard Lammel	
Report No. 336 January 2002	**An Improved Land Surface Parameter Dataset for Global and Regional Climate Models** Stefan Hagemann	
Report No. 337 May 2002	**Lidar intercomparisons on algorithm and system level in the frame of EARLINET** Volker Matthias, J. Bösenberg, H. Linné, V. Matthias, C. Böckmann, M. Wiegner, G. Pappalardo, A. Amodeo, V. Amiridis, D. Balis, C. Zerefos, A. Ansmann, I. Mattis, U. Wandinger, A. Boselli, X. Wang, A. Chaykovski, V. Shcherbakov, G. Chourdakis, A. Papayannis, A. Comeron, F. Rocadenbosch, A. Delaval, J. Pelon, L. Sauvage, F. DeTomasi, R. M. Perrone, R. Eixmann, J. Schneider, M. Frioud, R. Matthey, A. Hagard, R. Persson, M. Iarlori, V. Rizi, L. Konguem, S. Kreipl, G. Larchevêque, V. Simeonov, J. A. Rodriguez, D. P. Resendes, R. Schumacher	
Report No. 338 June 2002	**Intercomparison of water and energy budgets simulated by regional climate models applied over Europe** Stefan Hagemann, Bennert Machenhauer, Ole Bøssing Christensen, Michel Déqué, Daniela Jacob, Richard Jones, Pier Luigi Vidale * Climate Dynamics (submitted)	
Report No. 339 September 2002	**Modelling the wintertime response to upper tropospheric and lower stratospheric ozone anomalies over the North Atlantic and Europe** Ingo Kirchner, Dieter Peters	
Report No. 340 November 2002	**On the determination of atmospheric water vapour from GPS measurements** Stefan Hagemann, Lennart Bengtsson, Gerd Gendt * J. Geophys. Res., 2003, Vol. 108, No. D21, 4678	
Report No. 341 November 2002	**The impact of international climate policy on Indonesia** Armi Susandi, Richard S.J. Tol	
Report No. 342 December 2002	**Indonesian smoke aerosols from peat fires and the contribution from volcanic sulfur emissions** (only available as pdf-file on the web) Bärbel Langmann, Hans F. Graf	
Report No. 343 January 2003	**Modes of the wintertime Arctic temperature variability** Vladimir A. Semenov, Lennart Bengtsson	
Report No. 344 February 2003	**Indicators for persistence and long-range transport potential as derived from multicompartment chemistry-transport modelling** Adrian Leip, Gerhard Lammel	
Report No. 345 February 2003	**The early century warming in the Arctic – A possible mechanism** Lennart Bengtsson, Vladimir A. Semenov, Ola Johannessen	
Report No. 346 May 2003	**Variability of Indonesian Rainfall and the Influence of ENSO and Resolution in ECHAM4 Simulations and in the Reanalyses** Edvin Aldrian, Lydia Dümenil Gates, F. Heru Widodo	

MPI-Report-Reference: *Reprinted in

Report 1 - 302 Please order the reference list from MPI for Meteorology, Hamburg

Report No. 347
June 2003

Sensitivity of Large Scale Atmospheric Analyses to Humidity Observations and its Impact on the Global Water Cycle and Tropical and Extra-Tropical Weather Systems
L. Bengtsson, K. I. Hodges, S. Hagemann
* Tellus (accepted)

Report No. 348
September 2003

EARLINET: A European Aerosol Research Lidar Network to Establish an Aerosol Climatology
J. Bösenberg, V. Matthias, et al.

Report No. 349
November 2003

The atmospheric general circulation model ECHAM 5. PART I: Model description
E. Roeckner, G. Bäuml, L. Bonaventura, R. Brokopf, M. Esch, M. Giorgetta, S. Hagemann, I. Kirchner, L. Kornblueh, E. Manzini, A. Rhodin, U. Schlese, U. Schulzweida, A. Tompkins

Report No. 350
December 2003

Principles of variational assimilation of GNSS radio occulation data
M. E. Gorbunov, L. Kornblueh

Report No. 351
January 2004

Can Climate Trends be Calculated from Re-Analysis Data?
L. Bengtsson, S. Hagemann, K. I. Hodges

ISSN 0937 - 1060